

Disentangle Object and Non-object Infrared Features via Language Guidance

Fan Liu[†], Ting Wu, Chuanyi Zhang, Liang Yao, Xing Ma, Yuhui Zheng

Hohai University

[†]Corresponding Author

Email: fanliu@hhu.edu.cn

Abstract

Infrared object detection focuses on identifying and locating objects in complex environments (e.g., dark, snow, and rain) where visible imaging cameras are disabled by poor illumination. However, due to low contrast and weak edge information in infrared images, it is challenging to extract discriminative object features for robust detection. To deal with this issue, we propose a novel vision-language representation learning paradigm for infrared object detection. An additional textual supervision with rich semantic information is explored to guide the disentanglement of object and non-object features. Specifically, we propose a Semantic Feature Alignment (SFA) module to align the object features with the corresponding text features. Furthermore, we develop an Object Feature Disentanglement (OFD) module that disentangles text-aligned object features and non-object features by minimizing their correlation. Finally, the disentangled object features are entered into the detection head. In this manner, the detection performance can be remarkably enhanced via more discriminative and less noisy features. Extensive experimental results demonstrate that our approach achieves superior performance on two benchmarks: M^3FD (83.7% mAP), $FLIR$ (86.1% mAP). Our code will be publicly available once the paper is accepted.

1. Introduction

As a fundamental task in computer vision, object detection aims to identify and locate objects in images and videos. Unlike visible images, infrared ones are formed by thermal radiation, which can properly work under poor illumination. This advantage over RGB data allows infrared object detection (IROD) to have extensive applications in multiple scenarios, such as military reconnaissance [39], autonomous driving [51], and security surveillance [9].

Since the image-forming principles of visible and infrared images are different, they can provide complementary information. Therefore, a large number of works fuse

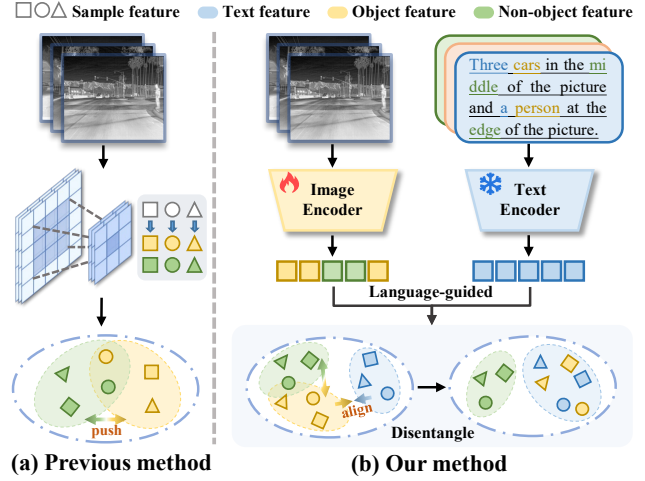


Figure 1. Comparison between previous method and our LGFD for feature disentanglement. (a) The previous method typically struggle to extract object features through convolution in an entangle feature space. (b) Our LGFD adopts a language-guided representation learning strategy. It disentangles the object and non-object feature via textual semantic information guidance.

visible and infrared images for detection [6, 13, 34, 45]. Nevertheless, obtaining precisely paired visible and infrared data has a high cost due to expensive dual-modality cameras and manual image matching. This drawback makes the infrared-visible fusion paradigms less practical.

Another branch of IROD research is merely utilizing infrared images without paired visible data. However, learning discriminative visual features from infrared images tends to be more challenging compared to learning from visible modality. Specifically, visible images have rich color and texture information, while infrared images primarily reflect the thermal radiation information of the object's surface rather than its visual appearance. Consequently, infrared images typically have low contrast and weak edge information due to inapparent texture and colorlessness. This trait makes it difficult to distinguish objects from the

background in infrared images. From this observation, it is intuitive to disentangle the object and background features to enhance the detection performance. The previous method [47] attempts to design feature extraction modules to separate object and background features. Nevertheless, merely relying on simple convolution modules to separate object features from global features without reliable supervision tends to result in an insufficient feature separation. Moreover, the extracted features of the object might lack interpretability.

Motivated by the previous object feature learning approach [47] (Figure 3 (a)), we aim to disentangle object and non-object features in an effective and interpretable manner. From the perspective of interpretability, utilizing image text descriptions with object categories and location information can provide semantic information of objects. The recent success of vision-language research [12, 14, 26] has proven the potential of text modality in representation learning. With the assistance of language, we can properly obtain object features via aligning visual and textual features.

To this end, we propose a **Language-guided Feature Disentanglement (LGFD)** approach to separate object and non-object features via the guidance of textual semantic information, as illustrated in Figure 3 (b). Through aligning text and object features, our LGFD can achieve more remarkable object and non-object feature disentanglement over the previous approach [47]. Specifically, we divide visual features channels into object and non-object groups. Then, we propose a Semantic Feature Alignment (SFA) module to align the object features with the corresponding text features. In this manner, we transform the conventional visual detection pipeline into a vision-language representation learning paradigm, enabling the detection model to learn semantic information from texts. The captions paired with the images are derived from the sample annotations and provide critical object semantic information. Moreover, we design an Object Feature Disentanglement (OFD) module that disentangles text-aligned object features and non-object features by minimizing the correlation between them. This essential disentanglement allows the model to focus on salient features relevant to the task while effectively reducing the influence of irrelevant non-object information. Finally, the disentangled object features are entered into the detection head. With noisy non-object information suppressed, the detection performance can be significantly boosted.

Our contributions are summarized as follows:

- We propose a novel vision-language representation learning paradigm that leverages textual semantic information to guide infrared object detection. To the best of our knowledge, **we are the first to investigate infrared image-text exploitation for detection tasks.**
- We develop an interpretable Language-guided Feature

Disentanglement framework. The proposed Semantic Feature Alignment (SFA) module learns object features from textual semantic information while the Object Feature Disentanglement (OFD) module enhances object features via decoupling non-object ones.

- We conduct comprehensive experiments on four infrared datasets to validate our method. Experimental results indicate that our approach surpasses all existing infrared object detection approaches and even outperforms many RGB-IR fusion detection frameworks.

2. Related Work

2.1. Infrared Object Detection

In recent years, object detection [40] models have effectively balanced performance in terms of speed and accuracy, *e.g.*, YOLO series [37] and DETR [24]. Some large-scale detectors [21, 28] have also demonstrated remarkable zero-shot detection performance. However, these methods [19] were typically proposed for object detection in visible images. Compared with well-developed visible domain, infrared object detection draws less attention from researchers. A common paradigm is to fine-tune visible image pre-trained detectors on infrared data [36, 49]. Nevertheless, due to the domain gap and different image-forming principles between visible and infrared images, models tend to show inferior performance on infrared data.

To enhance infrared object detection [13] and [6] developed multimodal networks that feed paired RGB and infrared samples into the network to detect objects in thermal images. However, obtaining paired images from both domains is difficult due to heavy manual image matching. Therefore, there existed several methods that aim to perform IROD without additional paired RGB data [30]. For example, [5] proposed a transfer learning approach called Source Model Guidance (SMG), which utilized high-capacity RGB detection models to guide and supervise the training of infrared detection networks. [47] designed the coordinate attention module to focus on objects and suppress the background. Although the above efforts made several progress, IROD performance still can be further improved.

2.2. Vision-language Representation Learning

Vision-language models (VLMs) have demonstrated significant potential in integrating visual and linguistic information [8, 11, 41, 42, 48]. They applied cross-modal pre-training and contrastive learning to obtain discriminative representation. For example, CLIP [26], ALIGN [12], and CyCLIP [10] achieved notable success in zero-shot image recognition tasks. Regarding other visual and linguistic tasks, Flamingo [1] utilized the visual and language inputs as prompts and showed remarkable few-shot performance for visual question answering. FLAVA [31] ad-

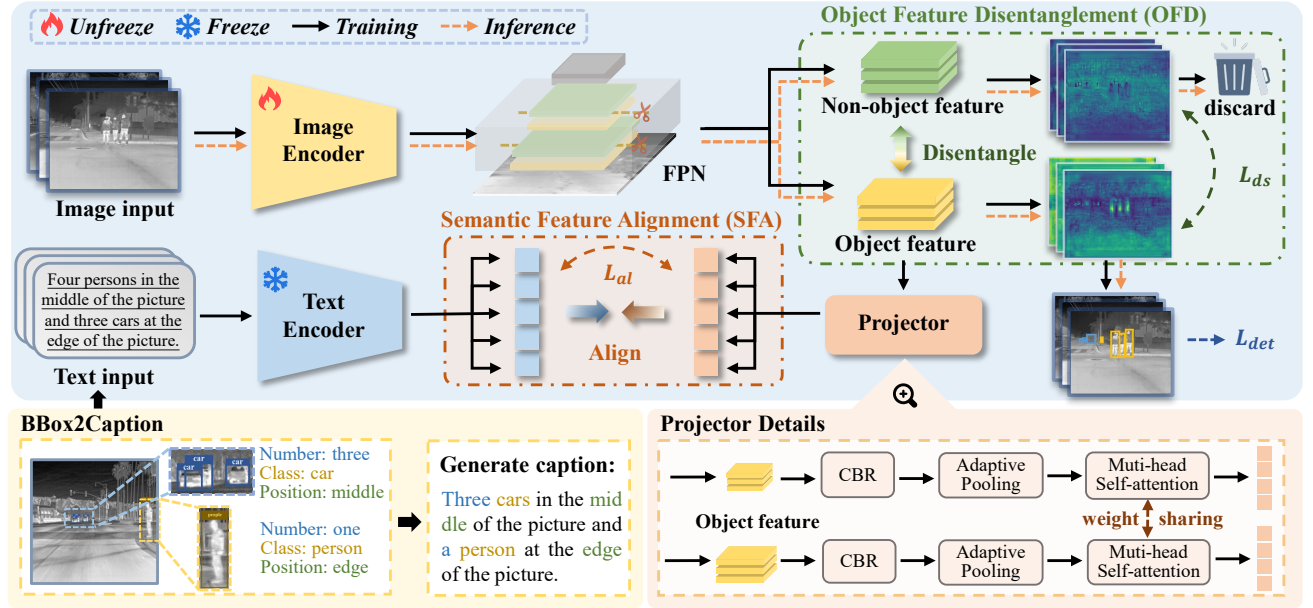


Figure 2. Our LGFD’s overall architecture. Initially, BBox2Caption is introduced to generate the detailed descriptions in a rule-based manner. The paired image-text data are entered into encoders to obtain features. Image FPN features are separated into object and non-object parts. Subsequently, the SFA module aligns object and text features to make the model learn semantic information pertinent to the objects. Meanwhile, the OFD module minimizes the similarity between the object and non-object features via a constraint loss. It can mitigate the influence of background on object feature extraction. Ultimately, the robust object features are leveraged to produce final detection output.

vanced multi-modality understanding by integrating visual and linguistic information, thereby improving performance in image classification and text retrieval. In the area of multi-modal retrieval, ALIGN [12] illustrated how contrastive learning can establish strong associations between images and texts, providing new insights for image-text retrieval tasks. BLIP [14] excelled in the interaction between images and texts, effectively conducting image-text matching and generation tasks. Motivated by the success of the above works in the vision-language field, our approach applies a vision-language representation learning paradigm to enhance IROD performance.

3. Proposed Method

In this section, we elaborate the proposed Language-guided Feature Disentanglement (LGFD) method, which is a novel vision-language representation learning paradigm for IROD. The overall framework is represented in Figure 2. To illustrate the process of disentangling the object feature and the non-object feature, we provided the Algorithm 1 of language guided feature disentanglement.

3.1. Problem Formulation

3.1.1. Revisiting Infrared Object Detection

The objective of the IROD task is to learn a mapping that generates the detection results y_i from a set of input infrared

samples x_i . This process can be formally represented as:

$$p(Y|X; \mathcal{M}_\theta) = \prod_{i=1}^N p(y_i|x_i; \mathcal{M}_\theta), \quad (1)$$

where $p(\cdot)$ represents the conditional probability. X and Y denote the input and output within the mapping, respectively. N is the sample number. \mathcal{M}_θ denotes the model with learnable parameters θ .

IROD typically involves classification and regression. The classification task identifies the category c_i^k of each object:

$$p(c_i^k | x_i; \mathcal{M}_\theta) = \Phi(\mathcal{F}(x_i; \mathcal{M}_\theta))^k, \quad (2)$$

where k represents the k^{th} object. $\Phi(\cdot)$ and $\mathcal{F}(\cdot)$ are the functions of classification and feature extraction, respectively.

The regression task aims to accurately predict the location of each object. Assuming that bounding box b_i^k follows Gaussian distribution in the regression model [29], the process can be modeled as:

$$p(b_i^k | x_i; \mathcal{M}_\theta) = \mathcal{N}(\hat{b}_i^k(x_i; \mathcal{M}_\theta), (\sigma_i^k)^2), \quad (3)$$

where k represents the k^{th} object. \hat{b}_i^k and σ^2 denote the predicted bounding box and variance. The output \hat{y}_i consists of both classification and regression predictions to provide the

detection results:

$$\hat{y}_i = \{p(c_i^k | x_i; \mathcal{M}_\theta), p(b_i^k | x_i; \mathcal{M}_\theta)\}. \quad (4)$$

Then, the final optimization for IROD task is expressed as the following process:

$$\arg \min_{\theta} \mathcal{L}_{det} = \sum_{i=1}^N (d_{det}(\hat{y}_i, y_i); \mathcal{M}_\theta), \quad (5)$$

where $d_{det}(\cdot)$ is defined as distance metric functions between predictions and ground truth labels.

3.1.2. Language-guided Detection Paradigm

Our proposed LGFD separates the object and non-object features through language guidance. By integrating text supervision, the typical infrared detection pipeline is transformed into an infrared vision-language representation learning paradigm. The input is expanded from the original single image x_i to a binary $(x_i, t_i)_{i=1}^N$, where t_i is the auxiliary caption. Then, the mapping process of LGFD can be expressed as follows:

$$p(Y|(X, T); \mathcal{M}_\theta) = \prod_{i=1}^N p(y_i|(x_i, t_i); \mathcal{M}_\theta), \quad (6)$$

where X , T , and Y represent the visual input, textual input, and detection results within the mapping, respectively.

LGFD disentangles the visual features into object and non-object features prior to detection head as:

$$f_i^{obj}, f_i^{nobj} = g(\mathcal{F}(x_i, t_i; \mathcal{M}_\theta)), \quad (7)$$

where f_i^{obj} and f_i^{nobj} are object and non-object features. $g(\cdot)$ denotes the disentangle function. The decoupled object features f_i^{obj} are entered into the detection head for subsequent predictions \hat{y}_i . Consequently, the optimization objective with parameters θ transitions from (5) to (8):

$$\arg \min_{\theta} \mathcal{L} = \sum_{i=1}^N ((d_{det}(\hat{y}_i, y_i) + d_{dis}(f_i^{obj}, f_i^{nobj}); \mathcal{M}_\theta), \quad (8)$$

where $d_{dis}(\cdot)$ is defined as distance metric functions between the extracted features, such as the cosine similarity or Euclidean distance. Minimizing the \mathcal{L} effectively integrates IROD performance enhancement and object feature disentanglement.

3.2. Auxiliary Captions Generation

Previous IROD methods are merely supervised by detection labels (categories and bounding boxes). Differently, our approach explores the possibility of leveraging supervisory information in an alternative manner. Specifically, we

Algorithm 1 LGFD

Require:

captions: Text data that matches the images,

\mathcal{M}_θ : Detector with parameter θ ,

$f_i^{ori} \in \mathbb{R}^{H \times W \times 2L}$: Feature map of P_3 and P_4 ,

\mathcal{L}_{det} , \mathcal{L}_{al} , \mathcal{L}_{ds} : The object detection loss, the alignment loss and the disentanglement loss.

for each training epoch **do**

for each training sample feature $x_{\mathcal{M}_\theta}^{ori}$ **do**

Decomposing feature maps of P_3 and P_4 .

$f_i^{obj}, f_i^{nobj} = \text{Decompose}(f_i^{ori}; \mathcal{M}_\theta)$

Obtain the textual feature.

$f_i^{text} = BERT(\text{captions})$

Projecting f_i^{obj} for calculating the similarity.

$\hat{f}_i^{obj} = \text{Projector}(f_i^{obj})$

$S_{ij} = \frac{\hat{f}_i^{obj} \cdot f_j^{text}}{\|\hat{f}_i^{obj}\| \|f_j^{text}\|}$

Optimize \mathcal{L} to find optimal f_i^{obj} .

$\mathcal{L}_{ds} = \cos(\text{Pooling}(f_i^{obj}), \text{Pooling}(f_i^{nobj}))$

$\mathcal{L}_{al} = -\frac{1}{b} \sum_{i=1}^b \log \frac{\exp(S_{ii}/\tau)}{\sum_{j=1}^b \exp(S_{ij}/\tau)}$

$\mathcal{L} = \mathcal{L}_{det} + \alpha \mathcal{L}_{al} + \beta \mathcal{L}_{ds}$

end for

end for

return Optimized detectotr \mathcal{M}_θ

utilize infrared image annotations to automatically generate descriptive captions, as depicted in Figure 2.

We adopt a rule-based approach, namely Bbox2Caption, to transfer the bounding box annotations into a set of natural language captions. Specifically, it initially computes the number of objects and subsequently integrates number, category, and spatial information to generate a caption that provides detailed object descriptions. When an object appears more than 10 times, a more generalized term (e.g., ‘a large number of’, ‘lots of’) is employed in place of the exact number to enhance the readability and variability of the captions. Finally, we generate an overall caption for each image, which contains detailed information of objects.

3.3. Infrared Object Feature Disentanglement

The object and non-object features entangled in the feature space can decrease the model performance. Therefore, we aim to disentangle them with the guidance of textual semantic information to facilitate detection.

3.3.1. Visual Feature Decomposition

We perform channel decomposition directly on the Feature Pyramid Network (FPN), partitioning the visual features extracted by the backbone into two distinct groups. The decomposition process can be expressed as:

$$f_i^{obj}, f_i^{nobj} = \text{Decompose}(f_i^{ori}; \mathcal{M}_\theta), \quad (9)$$

where $f_i^{obj} \in \mathbb{R}^{H \times W \times L}$ and $f_i^{nobj} \in \mathbb{R}^{H \times W \times L}$ are the two feature maps decomposed from $f_i^{ori} \in \mathbb{R}^{H \times W \times 2L}$. f_i^{ori} is the initial feature extracted by the model \mathcal{M}_θ . Subsequently, we should disentangle f_i^{obj} and f_i^{nobj} as completely as possible, making them learn object and non-object features respectively. Afterward, the object features will be utilized for robust infrared detection tasks, while the non-object features should be discarded as task-independent components.

3.3.2. Semantic Feature Alignment

We employ the contrastive learning strategy to make f_i^{obj} learn object feature in an interpretable manner. Specifically, the visual backbone is trained with image-text dataset $\mathcal{D} = (x_i, t_i)_{i=1}^N$ where the auxiliary text t_i is automatically generated as described in Section 3.2. Then, we apply a pre-trained text encoder (e.g., BERT [7]) to obtain text features $f_i^{text} \in \mathbb{R}^{1 \times L}$.

Contrastive learning [26] requires the dimensionality alignment between visual and textual features. Therefore, we design a projector to map the dimensionalities of decomposed object features f_i^{obj} and text features f_i^{text} :

$$\hat{f}_i^{obj} = \text{MultiHead}(\text{Pooling}(CBR(f_i^{obj}))), \quad (10)$$

where CBR represents a block composed of 1×1 convolution layer (C), a batch normalization layer (B) and a rectified linear unit (R). Then, an adaptive pooling is employed to dynamically adjust the feature dimensions. Next, a multi-head self-attention layer is adopted to capture complex dependencies. Ultimately, we can obtain projected object features \hat{f}_i^{obj} with dimensionality aligned to text features f_i^{text} .

Subsequently, the contrastive loss is utilized to align the dimension-matched object and text features in a unified feature space. This loss function facilitates \hat{f}_i^{obj} to learn the object relevant features from textual semantic information. Specifically, f_i^{text} and \hat{f}_i^{obj} are concatenated within a training batch of size b , forming two embedding groups $\{\hat{f}_1^{obj}, \hat{f}_2^{obj}, \dots, \hat{f}_b^{obj}\} \{f_1^{text}, f_2^{text}, \dots, f_b^{text}\} \in \mathbb{R}^{b \times L}$. Afterwards, we compute cosine similarities between visual and textual embedding groups:

$$S_{ij} = \frac{\hat{f}_i^{obj} \cdot f_j^{text}}{\|\hat{f}_i^{obj}\| \|\hat{f}_j^{text}\|}, \quad (11)$$

where S_{ij} denotes the similarity of i^{th} visual feature and j^{th} textual feature. Then, the contrastive loss is calculated on the similarity matrix, which prompts pull the matched image-text samples while pushing apart the mismatched samples. The loss is given by the following equation:

$$\mathcal{L}_{al} = -\frac{1}{b} \sum_{i=1}^b \log \frac{\exp(S_{ii}/\tau)}{\sum_{j=1}^b \exp(S_{ij}/\tau)}, \quad (12)$$

where τ is the temperature parameter. Ultimately, f_i^{obj} can effectively learn object features by establishing a strong correlation between visual features and the semantic information from auxiliary captions.

3.3.3. Object Feature Disentanglement

Although our SFA module ensures f_i^{obj} to learn the object features, f_i^{nobj} may still reserve a portion of the object features. In this situation, if x^{nobj} is discarded, it may negatively impact the detection performance. In order to guide f_i^{obj} to learn intact object features, an intuitive idea is to push f^{obj} and f^{nobj} apart to disentangle them. To accomplish this objective, we employ a constraint on f^{obj} and f^{nobj} to minimizes their similarity:

$$\mathcal{L}_{ds} = \cos(\text{Pooling}(f^{obj}), \text{Pooling}(f^{nobj})), \quad (13)$$

where \cos means the cosine similarity. An average pooling is adopted to reduce the dimensionality. In this manner, object and non-object features can be significantly disentangled in the feature space.

Finally, considering the alignment loss \mathcal{L}_{al} , the disentanglement loss \mathcal{L}_{ds} , and the object detection loss \mathcal{L}_{det} . Our overall training objective can be expressed as:

$$\mathcal{L} = \mathcal{L}_{det} + \alpha \mathcal{L}_{al} + \beta \mathcal{L}_{ds}, \quad (14)$$

where α and β represent the hyper-parameters to balance each loss.

The captions are auxiliary supervision in the training phase to enhance object feature extraction. In the inference, no additional caption information is required. Throughout both phases, the disentangled object features are fed into the detection head to produce final results, while non-object features are simply discarded. Furthermore, since non-object features are discarded, the model inference complexity slightly decreases.

4. Experiments

4.1. Experimental Settings

Datasets. The proposed model is evaluated on two publicly available datasets: (1) **FLIR** offers a challenging infrared object detection benchmark. We utilized the aligned version with more precise labeling as provided by [43]. The dataset includes 5,142 precisely aligned infrared-visible paired images with 4,129 and 1,013 samples assigned for training and testing, respectively. (2) **M³FD** comprises 4,200 pairs of visible and thermal images captured by on-board cameras [20]. Following the original setup of the dataset, we utilized 80% of the images for training and the remaining 20% images for evaluation.

Importantly, since we concentrated on investigating IROD without paired RGB images, we only selected the infrared data in the above datasets for training.

Table 1. Comparison on FLIR dataset with infrared-visible and infrared-only approaches.

Method	Backbone	<i>mAP</i>	<i>AP₅₀</i>
<i>Infrared-visible</i>			
GAFF (2021)	ResNet18	37.5	72.9
GAFF (2021)	VGG16	37.3	72.7
CFT (2021)	CFB	40.2	78.7
IGT (2023)	Swin-T-Tiny	43.6	85.0
CrossFormer (2024)	ViT	42.1	79.3
YOLO-Fusion (2024)	CSPDarknet	-	84.7
FD ² -Net (2024)	CSPDarknet	-	82.9
<i>Infrared-only</i>			
SSD (2016)	VGG16	29.6	65.5
Faster-RCNN (2016)	ResNet50	37.6	74.4
SMG-Y (2022)	-	-	77.0
YOLOv5m (2020)	CSPDarknet	-	81.9
YOLO-ACN (2020)	CSPDarknet	-	82.3
RGBT (2022)	-	-	82.9
YOLO-CIR (2023)	CSPDarknet	-	84.9
LGFDF (ours)	CSPDarknet	45.8	86.1

Experimental Details. We selected YOLOv7-L [38] as the base detector for our proposed LGFD. It is initialized with the MS-COCO[18] pre-trained weight. We utilized a widely-used BERT [7] model as our text encoder. To evaluate object detection performance, we selected the widely-adopted metrics, mean average precision *mAP* and average precision at 50 IoU threshold *AP₅₀*. Our framework is trained for 300 epochs with a batch size of 16. We fixed the random seed to 42 to ensure the reproducibility of the experiments. All experiments are conducted on an NVIDIA RTX 3090 GPU.

4.2. Main Results

Compared Methods. We compare our proposed LGFD with several SOTA works, including infrared-visible and infrared-only methods. **Infrared-visible** object detection approaches utilize paired visible and infrared images, including GAFF [44], CFT [25], CrossFormer [13], YOLO-Fusion [35], IGT [4], FD²-Net [15], RFN [3], DeFusion [33], TarDAL [20], IGNet [16], MetaF [46]. **Infrared-only** object detection methods merely leverage infrared samples without paired RGB data, including specifically SSD [22], Faster-RCNN [27], SMG-Y [5], YOLO-ACN [17], RGBT [36], YOLO-CIR [47], CenterNet2 [50], Sparse RCNN [32], YOLOv7-tiny [38], Swin Transformer [23].

Experiments on FLIR. We validated the effectiveness of LGFD on the FLIR dataset. From the experimental results in Table 1, it can be observed that in comparison to infrared-

Table 2. Comparison on M³FD dataset with infrared-visible and infrared-only methods.

Method	Backbone	<i>mAP</i>	<i>AP₅₀</i>
<i>Infrared-visible</i>			
RFN (2022)	CSPDarknet	53.2	79.4
TarDAL (2022)	CSPDarknet	54.1	80.6
DeFusion (2022)	CSPDarknet	54.1	80.8
IGNet (2023)	CSPDarknet	54.5	81.5
MetaF (2023)	CSPDarknet	56.5	81.6
FD ² -Net (2024)	CSPDarknet	-	83.5
<i>Infrared-only</i>			
Swin Transformer (2021)	-	41.9	72.6
CenterNet2 (2021)	ResNet50	42.4	65.3
Sparse RCNN (2021)	ResNet50	44.8	76.4
YOLOv7-tiny (2023)	CSPDarknet	48.4	78.1
LGFDF (ours)	CSPDarknet	51.7	83.7

only methods, ours obtains a 0.8% improvement in *AP₅₀* over the suboptimal method. More importantly, our method surpasses all infrared-visible methods. Specifically, compared to IGT [4], LGFD achieves significant performance gains of 2.7% and 0.7% on *mAP* and *AP₅₀*, respectively. Considering that our approach merely utilizes infrared images without paired visible data, its superior performance over infrared-visible methods significantly demonstrates the advantages of our approach.

To directly explain the superior performance of our approach, we visualized the feature activation map compared with the baseline detector (YOLOv7-L) in Figure 3. The results in columns (a-c) represent that our method exhibits stronger activations to the interest regions where the ground truth exists. Moreover, the baseline has false activations in Figure 3 (d-f), while ours overcomes this drawback. The reason is that our LGFD can discard non-object features via disentanglement, thereby reducing the risk of being misguided by false feature activations. To sum up, stronger true and fewer false feature activations can account for the significant performance improvements of our approach.

Experiments on M³FD. We presented the experimental results in Table 2. It can be observed from Table 2 that our proposed LGFD surpasses all mainstream state-of-the-art (SOTA) methods in *AP₅₀*. Specifically, compared with infrared-only methods, LGFD shows advantages over the second-best method in *AP₅₀* by 5.4% and in *mAP* by 2.7%. In comparison to infrared-visible detection frameworks, our LGFD also exhibits superior performance in the *AP₅₀*. Although it is inferior to some infrared-visible methods in *mAP*, we believe this phenomenon is reasonable because LGFD doesn't utilize visible images as auxiliary data.

The experiments on two datasets indicate that the proposed approach can effectively enhance infrared object de-

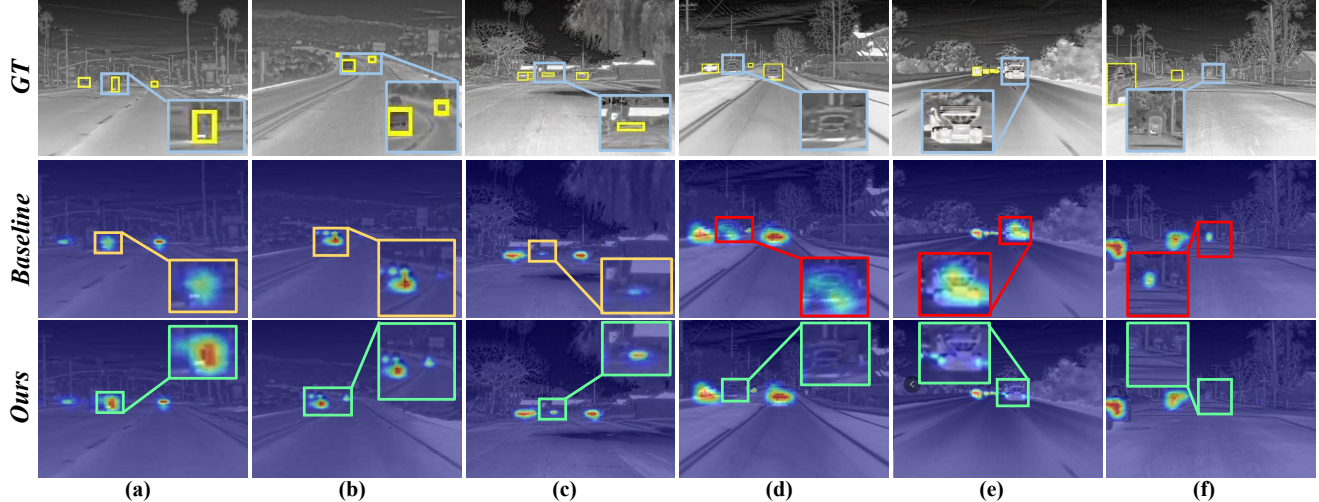


Figure 3. Visualization of feature activations results of our LGFD and baseline on FLIR with ground truth (GT). Orange (a-c) and red (d-f) boxes indicate weak and false activations, respectively. Green boxes represent the results of LGFD for comparison.

Table 3. Ablation study of LGFD components. SFA: Semantic feature alignment. OFD: Object feature disentanglement.

Dataset	SFA	OFD	<i>mAP</i>	<i>AP₅₀</i>	<i>AP₇₅</i>
FLIR	✓		44.2	84.2	39.5
		✓	45.3 (+1.1)	85.7 (+1.5)	40.6 (+1.1)
	✓	✓	45.2 (+1.0)	85.4 (+1.2)	39.7 (+0.2)
M ³ FD	✓		45.8 (+1.6)	86.1 (+1.9)	41.1 (+1.6)
		✓	47.6	78.3	49.0
	✓	✓	50.2 (+2.6)	82.9 (+4.6)	52.8 (+3.8)
		✓	51.1 (+3.5)	83.3 (+5.0)	53.0 (+4.0)
	✓	✓	51.7 (+4.1)	83.7 (+5.4)	53.3 (+4.3)

tection performance. Although it merely utilizes infrared data, it could even surpass infrared-visible detection methods. This satisfying result reveals the effectiveness of our vision-language representation learning paradigm and feature disentangling strategy for IROD.

4.3. Ablation Studies

4.3.1. Effectiveness of SFA and OFD Modules

Our method LGFD consists of two key components: Semantic Feature Alignment (SFA) and Object Feature Decoupling (OFD). Table 3 presents the effects of them for the final detection performance. It can be observed that the *AP₅₀* increases by 1.9% and 5.4% on the FLIR and M³FD respectively, when employing the SFA module. The incorporation of the OFD module further enhanced performance, leading to additional gains of 0.4% and 0.8% in *AP₅₀* on the two datasets. These results indicate that learning object features with language guidance significantly contributes to the final improvement (SFA). Additionally, the subsequent

Table 4. Impact of utilizing object features f^{obj} and non-object features f^{nobj} with YOLOv7 as the base detector.

Dataset	f^{obj}	f^{nobj}	<i>mAP</i>	<i>AP₅₀</i>	<i>AP₇₅</i>
FLIR	✓		44.2	84.2	39.5
		✓	45.8 (+1.6)	86.1 (+1.9)	41.1 (+1.6)
	✓	✓	44.3 (+0.1)	84.6 (+0.4)	39.2 (-0.3)
M ³ FD	✓		44.4 (+0.2)	82.8 (-1.4)	39.6 (+0.1)
		✓	47.6	78.3	49.0
	✓	✓	51.7 (+4.1)	83.7 (+5.4)	53.3 (+4.3)
		✓	49.3 (+1.7)	81.7 (+3.4)	51.1 (+2.1)
	✓	✓	51.3 (+3.7)	81.8 (+3.5)	52.1 (+3.1)

integration of disentangling object and non-object features can further boost the performance (OFD).

4.3.2. Impact of Object and Non-object Features

To obtain deeper insights into the disentangled features, we conducted experiments to validate the impact of object and non-object features on detection. Specifically, we enter the object feature and both object and non-object features into the detection head, respectively. As demonstrated in Table 4, utilizing f^{obj} effectively enhanced the performance by 5.4% and 1.9% of *AP₅₀* on two datasets compared to the baseline. However, if utilizing both f^{obj} and f^{nobj} features, the improvement over the baseline was decreased. The *AP₅₀* reductions are 3.3% and 1.9% on the FLIR and M³FD respectively. This result indicates that the non-object feature may contain detrimental information and discarding it can enhance the performance.

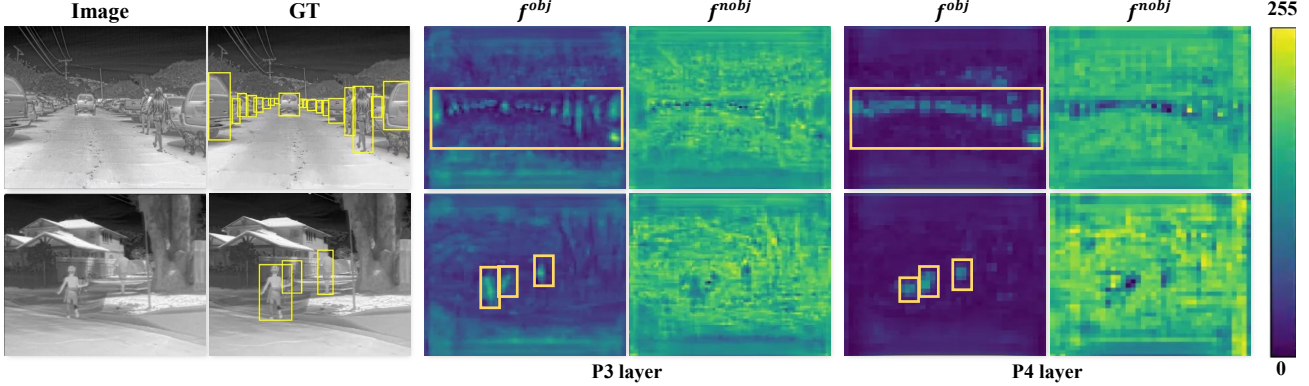


Figure 4. Visualization of object and non-object features of P3 and P4 layers in FPN. The object features are more focused on the foreground where the ground truth (GT) exists. Conversely, non-object features are primarily concerned with the background.

Table 5. The impact of decomposing different layers in FPN for the detection performance on FLIR dataset.

	P3	✓		✓	✓	✓
FPN	P4		✓	✓	✓	✓
	P5		✓	✓	✓	✓
AP_{50}	84.2	85.5	85.4	83.8	86.1	85.2
$\pm\Delta$	-	+1.3	+1.2	-0.4	+1.9	+1.0
					0.0	-0.2

4.3.3. Feature Disentanglement Visualization

To investigate the feature representation capabilities of the proposed LGFD, we conducted a visual analysis of the object and non-target features after disentangling the P3 and P4 layers of FPN. As illustrated in Figure 4, it is evident that LGFD significantly disentangles the features into object and non-object components. The high-response regions of f^{obj} and f^{nonobj} correspond to the foreground and background respectively. Therefore, the effectiveness of LGFD lies in its ability to concentrate on robust object features while suppressing background noise.

4.3.4. Decomposition at Different FPN Layers

We explore the effectiveness of disentanglement at different locations through experiments conducted on various resolution layers of the FPN. The results are presented in Table 5, and the best performance are achieved by disentangling at the P3 and P4 layers. The reason could be that the proportion of large-scale objects, which P5 layers detects, in the two datasets is relatively small, accounting for about 7% and 11%, respectively. Consequently, we ultimately choose to disentangle the P3 and P4 layers that correspond to detect small and medium-scale objects, with a significant improvement of 1.9% on the P3 and P4 layers.

Table 6. The impact of different caption generation strategies on the two datasets.

Dataset	Method	mAP	AP_{50}	AP_{75}
FLIR	no-caption	44.2	84.2	39.5
	LVLMs-based	45.3	85.5	40.8
	rule-based	45.8	86.1	41.1
M^3FD	no-caption	47.6	78.3	49.0
	LVLMs-based	51.2	83.4	53.1
	rule-based	51.7	83.7	53.3

4.3.5. Different Caption Generation Approaches

To select a proper caption generation method, we compared the Large Vision-Language Model (LVLMs-based) by Qwen-VL [2] and the rule-based method. The results are illustrated in Table 6. We can observe that text supervision is effective. Furthermore, the rules-based method surpasses LVLMs-based method by 0.6% and 0.3% on AP_{50} on the FLIR and M^3FD , respectively. This phenomenon is mainly attributed to the fact that the typical LVLM is not optimized for infrared modality and the hallucination problem tends to provide fake information. Therefore, we adopt simple yet effective rule-based caption generation.

5. Conclusion

In this paper, we proposed a Language-Guided Feature Disentanglement (LGFD) approach specifically designed for infrared object detection tasks. It effectively separates object and non-object features by incorporating semantic language guidance. SFA module achieves effective feature disentanglement through the alignment of object features with corresponding textual features. OFD module ensures that the model can focus on object features while minimizing the impact of non-object features. By converting the detection pipeline into a vision-language representation learn-

ing framework, LGFD significantly enhances infrared object detection performance. Experiments demonstrate the effectiveness of integrating semantic information from text modality. In future work, we will further investigate the potential of LGFD in other multimodal perception tasks.

References

- [1] Jean-Baptiste Alayrac, Jeff Donahue, Pauline Luc, Antoine Miech, Iain Barr, Yana Hasson, Karel Lenc, Arthur Mensch, Katherine Millican, Malcolm Reynolds, et al. Flamingo: a visual language model for few-shot learning. *NeurIPS*, 35: 23716–23736, 2022. [2](#)
- [2] Jinze Bai, Shuai Bai, Yunfei Chu, Zeyu Cui, Kai Dang, Xiaodong Deng, Yang Fan, Wenbin Ge, Yu Han, Fei Huang, et al. Qwen technical report. *arXiv preprint arXiv:2309.16609*, 2023. [8](#)
- [3] Ting-Jui Chang and Shahin Shahrampour. Rfn: A random-feature based newton method for empirical risk minimization in reproducing kernel hilbert spaces. *TSP*, 70:5308–5319, 2022. [6](#)
- [4] Keyu Chen, Jinqiang Liu, and Han Zhang. Igt: Illumination-guided rgb-t object detection with transformers. *Knowledge-Based Systems*, 268:110423, 2023. [6](#)
- [5] Ruimin Chen, Shijian Liu, Jing Mu, Zhuang Miao, and Fanning Li. Borrow from source models: efficient infrared object detection with limited examples. *Applied Sciences*, 12(4):1896, 2022. [2, 6](#)
- [6] Yishuo Chen, Boran Wang, Xinyu Guo, Wenbin Zhu, Jia-sheng He, Xiaobin Liu, and Jing Yuan. Deyolo: Dual-feature-enhancement yolo for cross-modality object detection. In *ICPR*, pages 236–252, 2025. [1, 2](#)
- [7] Jacob Devlin. Bert: Pre-training of deep bidirectional transformers for language understanding. *arXiv*, 2018. [5, 6](#)
- [8] Yu Du, Fangyun Wei, Zihe Zhang, Miaojing Shi, Yue Gao, and Guoqi Li. Learning to prompt for open-vocabulary object detection with vision-language model. In *CVPR*, pages 14084–14093, 2022. [2](#)
- [9] Indah Monisa Firdiantika and Sungho Kim. One-stage infrared ships detection with attention mechanism. In *ICCAS*, pages 448–451, 2023. [1](#)
- [10] Shashank Goel, Hritik Bansal, Sumit Bhatia, Ryan Rossi, Vishwa Vinay, and Aditya Grover. Cyclip: Cyclic contrastive language-image pretraining. *NeurIPS*, 35:6704–6719, 2022. [2](#)
- [11] Jiho Jang, Chaerin Kong, Donghyeon Jeon, Seonhoon Kim, and Nojun Kwak. Unifying vision-language representation space with single-tower transformer. In *AAAI*, pages 980–988, 2023. [2](#)
- [12] Chao Jia, Yinfei Yang, Ye Xia, Yi-Ting Chen, Zarana Parekh, Hieu Pham, Quoc Le, Yun-Hsuan Sung, Zhen Li, and Tom Duerig. Scaling up visual and vision-language representation learning with noisy text supervision. In *ICML*, pages 4904–4916, 2021. [2, 3](#)
- [13] Seungik Lee, Jaehyeong Park, and Jinsun Park. Cross-former: Cross-guided attention for multi-modal object detection. *PRL*, 179:144–150, 2024. [1, 2, 6](#)
- [14] Junnan Li, Dongxu Li, Caiming Xiong, and Steven Hoi. Blip: Bootstrapping language-image pre-training for unified vision-language understanding and generation. In *ICML*, pages 12888–12900, 2022. [2, 3](#)
- [15] Ke Li, Di Wang, Zhangyuan Hu, Shaofeng Li, Weiping Ni, Lin Zhao, and Quan Wang. Fd2-net: Frequency-driven feature decomposition network for infrared-visible object detection. *arXiv*, 2024. [6](#)
- [16] Pei Li, Sheng Wang, Hantao Zhao, Jia Yu, Liyang Hu, Haodong Yin, and Zhiyuan Liu. Ig-net: An interaction graph network model for metro passenger flow forecasting. *TITS*, 24(4):4147–4157, 2023. [6](#)
- [17] Yongjun Li, Shasha Li, Haohao Du, Lijia Chen, Dongming Zhang, and Yao Li. Yolo-acn: Focusing on small target and occluded object detection. *IEEE access*, 8:227288–227303, 2020. [6](#)
- [18] Tsung-Yi Lin, Michael Maire, Serge Belongie, James Hays, Pietro Perona, Deva Ramanan, Piotr Dollár, and C Lawrence Zitnick. Microsoft coco: Common objects in context. In *ECCV*, pages 740–755, 2014. [6](#)
- [19] Fan Liu, Liang Yao, Chuanyi Zhang, Ting Wu, Xinlei Zhang, Xiruo Jiang, and Jun Zhou. Boost uav-based object detection via scale-invariant feature disentanglement and adversarial learning. *IEEE TGRS*, 2025. [2](#)
- [20] Jinyuan Liu, Xin Fan, Zhanbo Huang, Guanyao Wu, Risheng Liu, Wei Zhong, and Zhongxuan Luo. Target-aware dual adversarial learning and a multi-scenario multi-modality benchmark to fuse infrared and visible for object detection. In *CVPR*, pages 5802–5811, 2022. [5, 6](#)
- [21] Shilong Liu, Zhaoyang Zeng, Tianhe Ren, Feng Li, Hao Zhang, Jie Yang, Chunyuan Li, Jianwei Yang, Hang Su, Jun Zhu, et al. Grounding dino: Marrying dino with grounded pre-training for open-set object detection. *arXiv*, 2023. [2](#)
- [22] Wei Liu, Dragomir Anguelov, Dumitru Erhan, Christian Szegedy, Scott Reed, Cheng-Yang Fu, and Alexander C Berg. Ssd: Single shot multibox detector. In *ECCV*, pages 21–37, 2016. [6](#)
- [23] Ze Liu, Yutong Lin, Yue Cao, Han Hu, Yixuan Wei, Zheng Zhang, Stephen Lin, and Baining Guo. Swin transformer: Hierarchical vision transformer using shifted windows. In *ICCV*, pages 10012–10022, 2021. [6](#)
- [24] Yifan Pu, Weicong Liang, Yiduo Hao, Yuhui Yuan, Yukang Yang, Chao Zhang, Han Hu, and Gao Huang. Rank-detr for high quality object detection. *NeurIPS*, 36, 2024. [2](#)
- [25] Fang Qingyun, Han Dapeng, and Wang Zhaokui. Cross-modality fusion transformer for multispectral object detection. *arXiv*, 2021. [6](#)
- [26] Alec Radford, Jong Wook Kim, Chris Hallacy, Aditya Ramesh, Gabriel Goh, Sandhini Agarwal, Girish Sastry, Amanda Askell, Pamela Mishkin, Jack Clark, et al. Learning transferable visual models from natural language supervision. In *ICML*, pages 8748–8763, 2021. [2, 5](#)
- [27] Shaoqing Ren, Kaiming He, Ross Girshick, and Jian Sun. Faster r-cnn: Towards real-time object detection with region proposal networks. *TPAMI*, 39(6):1137–1149, 2016. [6](#)
- [28] Tianhe Ren, Yihao Chen, Qing Jiang, Zhaoyang Zeng, Yuda Xiong, Wenlong Liu, Zhengyu Ma, Junyi Shen, Yuan Gao,

Xiaoke Jiang, et al. Dino-x: A unified vision model for open-world object detection and understanding. *arXiv*, 2024. 2

[29] T-YLPG Ross and GKHP Dollár. Focal loss for dense object detection. In *CVPR*, pages 2980–2988, 2017. 3

[30] Manish Sharma, Moitreya Chatterjee, Kuan-Chuan Peng, Suhas Lohit, and Michael Jones. Tensor factorization for leveraging cross-modal knowledge in data-constrained infrared object detection. In *ICCV*, pages 924–932, 2023. 2

[31] Amanpreet Singh, Ronghang Hu, Vedanuj Goswami, Guillaume Couairon, Wojciech Galuba, Marcus Rohrbach, and Douwe Kiela. Flava: A foundational language and vision alignment model. In *CVPR*, pages 15638–15650, 2022. 2

[32] Peize Sun, Rufeng Zhang, Yi Jiang, Tao Kong, Chenfeng Xu, Wei Zhan, Masayoshi Tomizuka, Lei Li, Zehuan Yuan, Changhu Wang, et al. Sparse r-cnn: End-to-end object detection with learnable proposals. In *CVPR*, pages 14454–14463, 2021. 6

[33] Yiming Sun, Bing Cao, Pengfei Zhu, and Qinghua Hu. Det-fusion: A detection-driven infrared and visible image fusion network. In *ACM MM*, pages 4003–4011, 2022. 6

[34] Hao Tang, Zechao Li, Dong Zhang, Shengfeng He, and Jin-hui Tang. Divide-and-conquer: Confluent triple-flow network for rgb-t salient object detection. *TPAMI*, 2024. 1

[35] Jun Tang, Caixian Ye, Xianlai Zhou, and Lijun Xu. Yolo-fusion and internet of things: Advancing object detection in smart transportation. *Alexandria Engineering Journal*, 107: 1–12, 2024. 6

[36] Sam Vadidar, Ali Kariminezhad, Christian Mayr, Laurent Kloeker, and Lutz Eckstein. Robust environment perception for automated driving: A unified learning pipeline for visual-infrared object detection. In *IV*, pages 367–374, 2022. 2, 6

[37] Ao Wang, Hui Chen, Lihao Liu, Kai Chen, Zijia Lin, Jun-gong Han, and Guiguang Ding. Yolov10: Real-time end-to-end object detection. *arXiv*, 2024. 2

[38] Chien-Yao Wang, Alexey Bochkovskiy, and Hong-Yuan Mark Liao. Yolov7: Trainable bag-of-freebies sets new state-of-the-art for real-time object detectors. In *CVPR*, pages 7464–7475, 2023. 6

[39] Song Xue, Yongfeng Liu, Chao Xu, and Jun Li. Object detection in visible and infrared missile borne fusion image. In *ICIML*, pages 19–23, 2022. 1

[40] Liang Yao, Fan Liu, Chuanyi Zhang, Zhiqian Ou, and Ting Wu. Domain-invariant progressive knowledge distillation for uav-based object detection. *IEEE GRSL*, 2024. 2

[41] Liang Yao, Fan Liu, Delong Chen, Chuanyi Zhang, Yijun Wang, Ziyun Chen, Wei Xu, Shimin Di, and Yuhui Zheng. Remotesam: Towards segment anything for earth observation. In *ACM MM*, pages 3027–3036, 2025. 2

[42] Liang Yao, Fan Liu, Hongbo Lu, Chuanyi Zhang, Rui Min, Shengxiang Xu, Shimin Di, and Pai Peng. Remotereasoner: Towards unifying geospatial reasoning workflow. *arXiv preprint arXiv:2507.19280*, 2025. 2

[43] Heng Zhang, Elisa Fromont, Sébastien Lefèvre, and Bruno Avignon. Multispectral fusion for object detection with cyclic fuse-and-refine blocks. In *ICIP*, pages 276–280, 2020. 5

[44] Heng Zhang, Elisa Fromont, Sébastien Lefèvre, and Bruno Avignon. Guided attentive feature fusion for multispectral pedestrian detection. In *WACV*, pages 72–80, 2021. 6

[45] Ruiheng Zhang, Zhe Cao, Yan Huang, Shuo Yang, Lixin Xu, and Min Xu. Visible-infrared person re-identification with real-world label noise. *TCSV7*, 2025. 1

[46] Wenda Zhao, Shigeng Xie, Fan Zhao, You He, and Huchuan Lu. Metafusion: Infrared and visible image fusion via meta-feature embedding from object detection. In *CVPR*, pages 13955–13965, 2023. 6

[47] Jinjie Zhou, Baohui Zhang, Xilin Yuan, Cheng Lian, Li Ji, Qian Zhang, and Jiang Yue. Yolo-cir: The network based on yolo and convnext for infrared object detection. *Infrared Physics & Technology*, 131:104703, 2023. 2, 6

[48] Kaiyang Zhou, Jingkang Yang, Chen Change Loy, and Ziwei Liu. Learning to prompt for vision-language models. *IJCV*, 130(9):2337–2348, 2022. 2

[49] Tong Zhou, Zhentao Yu, Yu Cao, Hongyang Bai, and Yan Su. Study on an infrared multi-target detection method based on the pseudo-two-stage model. *Infrared Physics & Technology*, 118:103883, 2021. 2

[50] Xingyi Zhou, Vladlen Koltun, and Philipp Krähenbühl. Probabilistic two-stage detection. *arXiv*, 2021. 6

[51] Xiaopei Zhu, Yuqiu Liu, Zhanhao Hu, Jianmin Li, and Xiaolin Hu. Infrared adversarial car stickers. In *CVPR*, pages 24284–24293, 2024. 1

Disentangle Object and Non-object Infrared Features via Language Guidance

Supplementary Material

1. Additional Ablation Studies

1.1. Effect of Balance Factors

To ascertain the optimal balance factor values for model training, we conducted experiments on M³FD with different weights for the hyper-parameter α and β . The results are demonstrated in Table 1. Models were trained using various parameter settings and the mean average precision (*mAP*) was recorded at the 50th epoch to save experiment time. It is evident that increasing or decreasing the weight α of aligning loss \mathcal{L}_{al} significantly impacts the model's detection performance. This result reflects the importance of learning object features from the textual information.

The accuracy tends to decrease when the weight β of disentangling loss \mathcal{L}_{ds} exceeds α . The reason may be that excessive disentanglement can weaken the strength of learning object features from semantic language guidance. Additionally, the detection accuracy may also be inferior when the disparity between the two balance factors is relatively large. This phenomenon suggests that balanced weights allocation can lead to superior model performance. Consequently, we ultimately adopt the set of balance factors of the highest accuracy in LGFD.

1.2. Analysis of CBR Block in Projector

We conducted experiments on the FLIR and M³FD datasets to validate the optimal choice of projector, including the number and size of convolution kernels in the CBR blocks. The results are demonstrated in Table 2 and Table 4. We selected CBR blocks with convolution kernel sizes of 1 and 3 to align feature dimensions (channels) for feature extraction. The results indicated that our LGFD achieved the best performance with a 1×1 convolution kernel in CBR block. Compared to scenarios without CBR blocks, this approach yielded performance gains of 2.3% and 0.5% in *AP*₅₀ on the FLIR and M³FD datasets, respectively. Therefore, in all experiments we utilized CBR blocks with a 1×1 convolution kernel to achieve optimal performance.

1.3. Detailed Detection Results

We compared the performance of our proposed method LGFD with the base detector YOLOv7-L as baseline on two IROD benchmark datasets. The detailed results are demonstrated in Table 3 with *AP*_S, *AP*_M, and *AP*_L as additional elevation metrics.

From the results in Table 3, we can observed that *AP*_S to *AP*_L all rises on two datasets. This phenomenon means that our approach can consistently improve the detection result across different scales. Specifically, on the M³FD dataset,

Table 1. Hyper-parameter analysis of weights α and β on M³FD. Balanced weights produces the best performance.

α	β	<i>mAP</i>	<i>AP</i> ₅₀	<i>AP</i> ₇₅
0.5×	1.5×	42.0	68.3	42.8
1.5×	0.5×	44.9	72.8	45.6
1.0×	0.5×	45.3	74.6	45.9
0.5×	1.0×	43.7	71.9	44.1
1.0×	1.0×	47.4	75.9	49.3

Table 2. Analysis of convolution kernels with different numbers and sizes in CBR block on FLIR.

Kernel	Person	Car	Bicycle	<i>AP</i> ₅₀
-	90.1	89.1	72.3	83.8
[1 × 1]	90.2	92.5	75.6	86.1
[3 × 3]	88.6	92.0	73.9	84.8
[3 × 3] × 2	89.2	92.1	74.6	85.3

Table 3. Comparison of *AP* on three benchmark datasets by utilizing our approach with the base detectors YOLOv7. Our approach effectively improves detection accuracy across different datasets.

Datasets	Method	<i>mAP</i>	<i>AP</i> ₅₀	<i>AP</i> ₇₅	<i>AP</i> _S	<i>AP</i> _M	<i>AP</i> _L
FLIR	baseline	44.2	84.2	39.5	32.3	49.3	64.3
	ours	45.8	86.1	41.1	34.6	50.7	66.8
	$\pm\Delta$	+1.6	+1.9	+1.6	+2.3	+1.4	+2.5
M ³ FD	baseline	47.6	78.3	49.0	19.0	59.1	79.7
	ours	51.7	83.7	53.3	25.4	62.0	80.4
	$\pm\Delta$	+4.1	+5.4	+4.3	+6.4	+2.8	+0.7

Table 4. Analysis of convolution kernels with different numbers and sizes in CBR block on M³FD.

Kernel	Bus	Car	Lamp	Truck	<i>AP</i> ₅₀
-	89.4	91.2	70.8	87.4	83.2
[1 × 1]	88.5	90.9	71.7	87.4	83.7
[3 × 3]	86.8	90.7	69.3	85.6	82.7
[3 × 3] × 2	87.3	90.3	70.2	86.8	83.1

the detection performance on small objects (*AP*_S) remarkably enhanced by +6.4%. Since small objects tend to be more difficult to detect, the improvement on them can support the effectiveness of our approach.

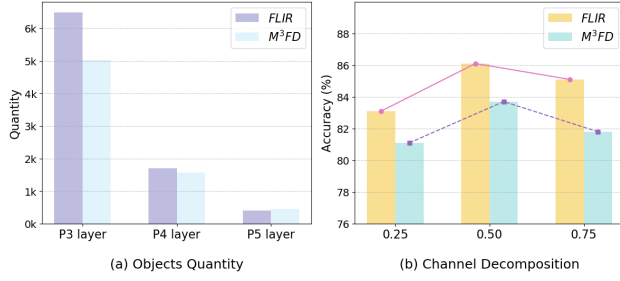


Figure 1. Statistical analysis of objects quantity and sensitivity analysis of channel decomposition. (a) The quantity of objects is calculated from different FPN layers on the two datasets. (b) The horizontal axis represents the proportion of decomposed object feature compared to the original feature.

1.4. Objects Quantity at Different FPN Layers

We count the quantities of objects from each detection head. As illustrated in Figure 1 (a), the proportion of large-scale objects (P5 layer detects) in the two datasets is relatively small, accounting for about 7% and 11% of the total number of objects on the two datasets, respectively. Consequently, we ultimately choose to disentangle the P3 and P4 layers that correspond to detect small and medium-scale objects. And our method achieves a significant improvement of 1.92% on the P3 and P4 layers.

1.5. Channel Decomposition Sensitivity Analysis

The original features were divided into object features and non-object features. To investigate the impact of channel decomposition ratio on the final detection performance, we conduct experiments with the ratio set at 0.25, 0.5, and 0.75, respectively. The results are illustrated in Figure 1 (b). The best performance was achieved when the object features accounted for half of the original features. Accordingly, we adopted an even split of the original feature channels.

1.6. Different Captions Generation Approaches

We generate the natural-language descriptions of infrared images employing the Qwen-VL model. However, there are many noisy captions with Figure 2 as an example. This phenomenon is mainly attributed to the fact that the typical LVL is not optimized for infrared modality and the hallucination problem tends to provide fake information. Furthermore, our approach still works with weakly supervised noisy captions. It can be extended to scenarios where detailed annotations are unavailable.

2. Visual Analysis

We visualized more object detection results on FLIR that we could not include in the main paper. From the visualization results in Figure 3, the LGFD significantly disentangles the features into object and non-object components

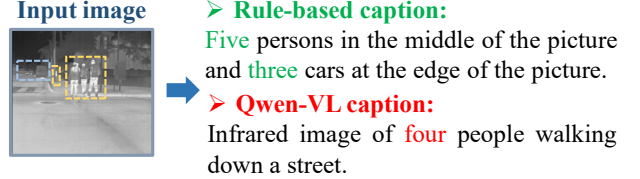


Figure 2. An example of natural-language description.

which split by P3 and P4 layers of FPN. Therefore, we can conclude that the effectiveness of LGFD lies in its ability to concentrate on robust object features while suppressing background noise.

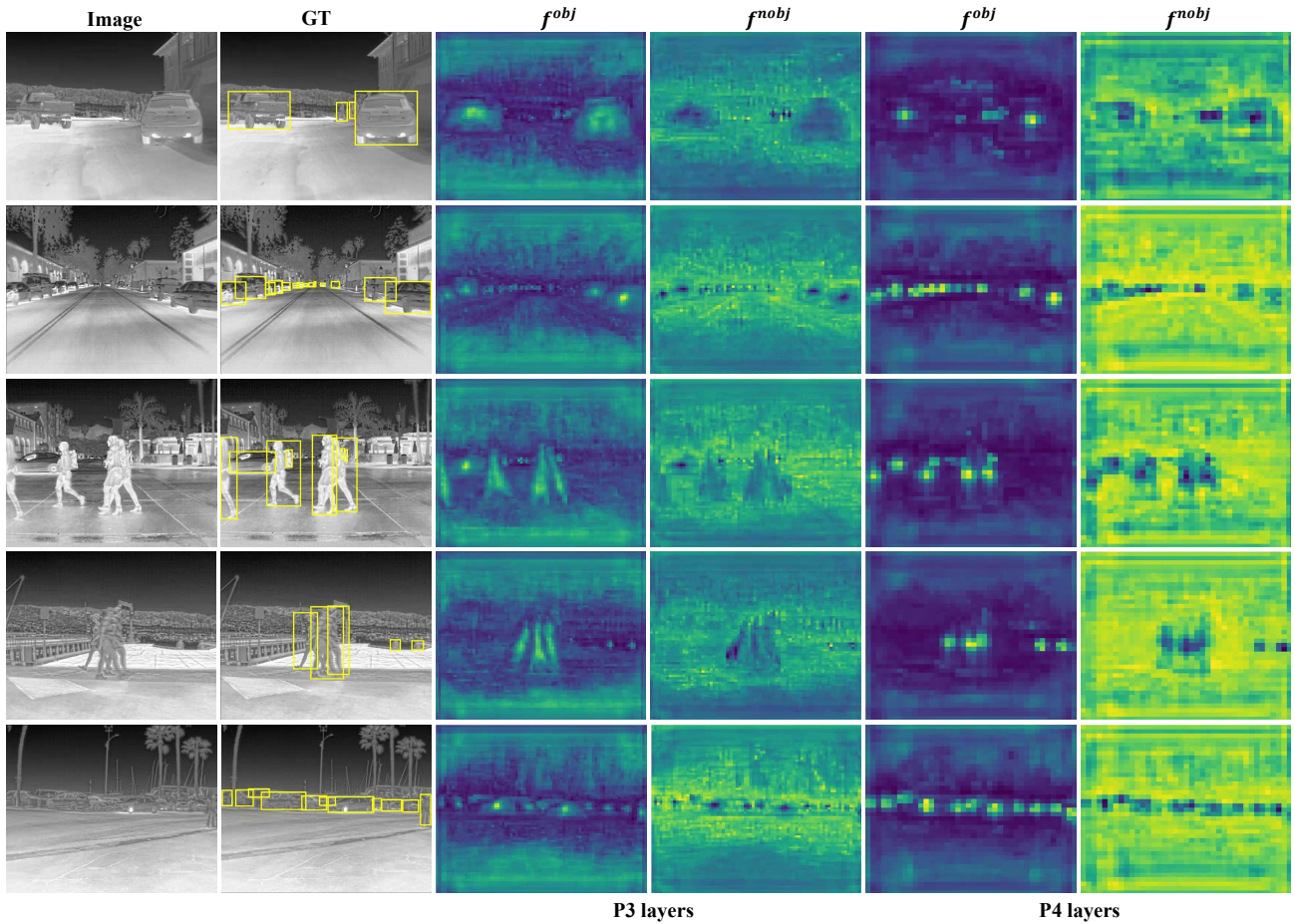


Figure 3. Visualization of object and non-object features of P3 and P4 layers in FPN. The object features are more focused on the foreground where the ground truth (GT) exists. Conversely, non-object features are primarily concerned with the background.